Electronic Supplementary Material (ESI) for Materials Horizons.

Supplementary Information for

Fracture-controlled surfaces as extremely durable ice-shedding materials

Sina Nazifi[1], Zixu Huang[1], Alireza Hakimian[1] and Hadi Ghasemi[1,2*]

[1]Department of Mechanical Engineering, University of Houston, 4726 Calhoun Rd, Houston, Texas 77204, USA
[2]Department of Chemical and Biomolecular Engineering, University of Houston, 4726 Calhoun Rd, Houston, Texas 77204, USA

*Correspondence to: hghasemi@uh.edu.

Supplementary Figures

Supplementary Figure 1. FCS sample preparation. a) Synthesis procedure of FCS is schematically shown here and explained in detail in **Supplementary Note 1.** b) FCS material is applied with 100 µm thickness on a glass substrate, c) Static water contact angle on FCS, d) Contact angle hysteresis on FCS.

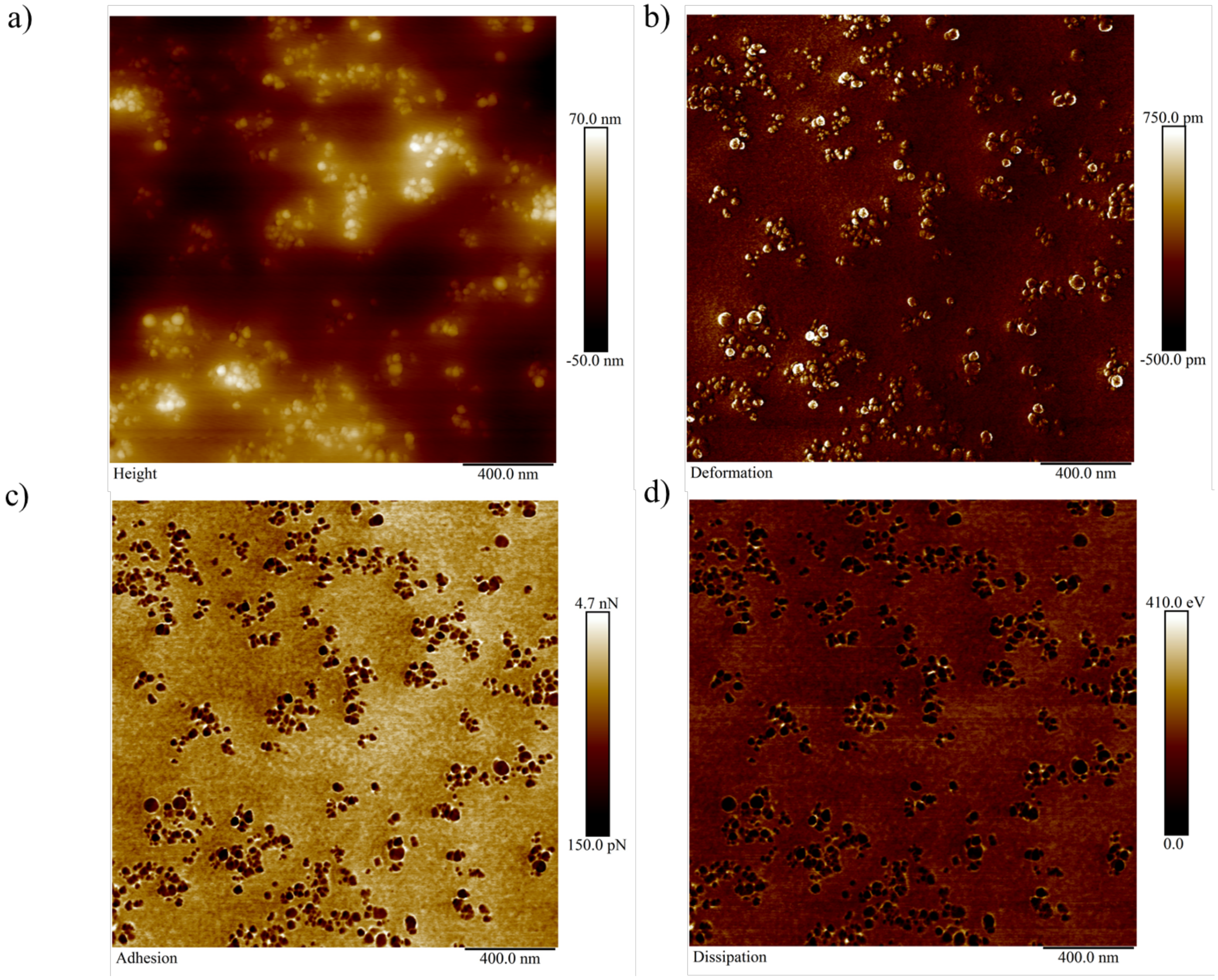

Supplementary Figure 2. Surface morphology of FCS. (a) Height map of FCS sample is shown. The gel-rich-sites are elevated approximately 50 nm higher. Also, the dimension of the gel and silica particles are $500\ nm$ and $20\ nm$ respectively. (b) Deformation of the AFM tip while scanning the surface is shown. The higher tip deformation indicates a higher modulus of the contacted surface. (c) The adhesion force of the AFM tip to the sample is shown. It represents minimal adhesion on hydrophobic silica sites which is important for effectively promoting the crack growth and detachment. (d) Dissipated energy between the AFM tip and the sample is suggesting minimal energy dissipation in silica-rich sites. That is essential for fast crack growth in phase III.

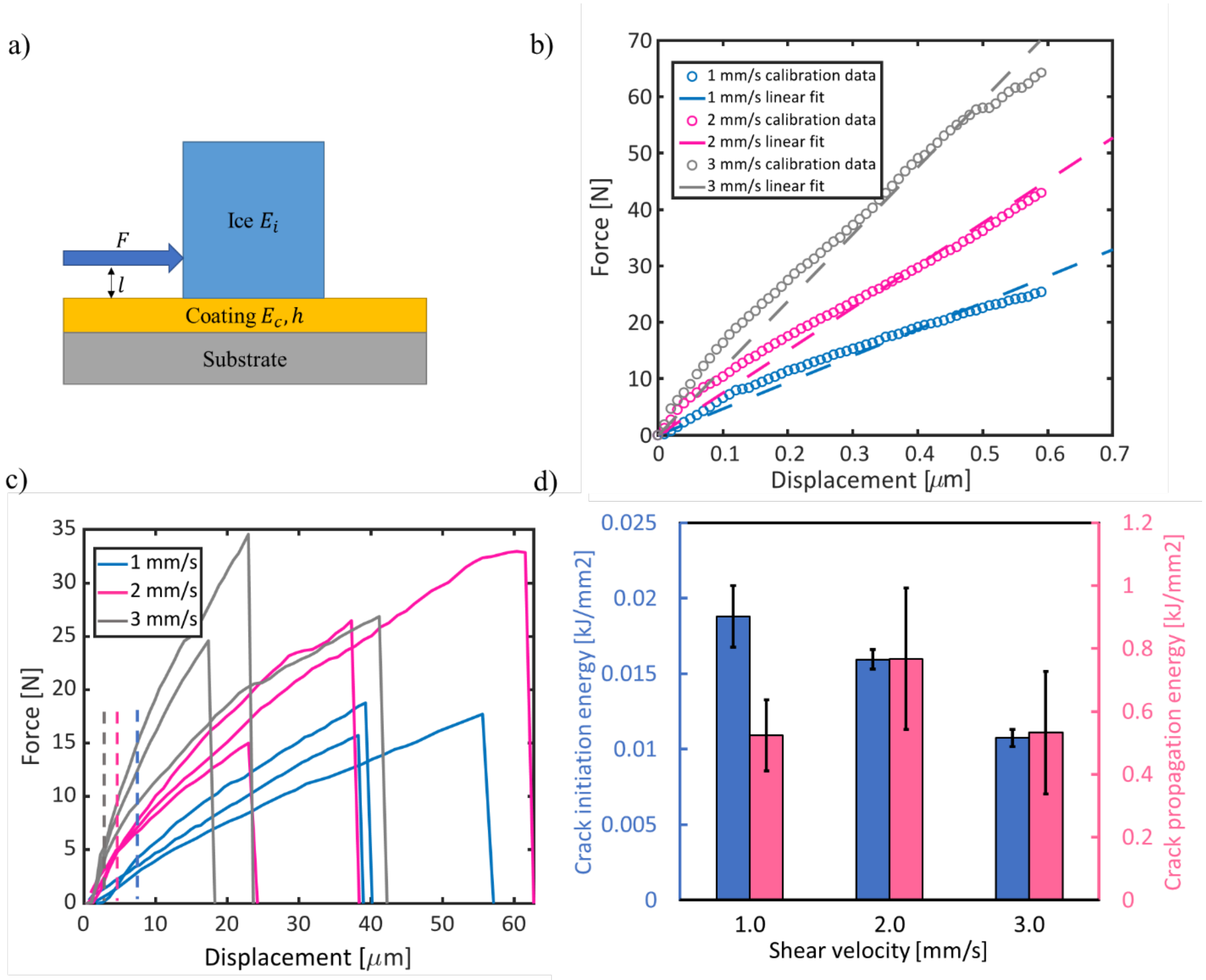

Supplementary Figure 3. Ice adhesion setup. (a) Schematic of ice adhesion setup is presented. (b) Calibration data collection for displacements of the setup as the force gauge keeps pushing a rigid body of the same size glued to the substrate on the cold plate at different shear rates. A linear fit is used in order to subtract displacement for a designated force in the experiment in **Fig. 1b**. Linear fit is the best model for such a system since all the displacements in the system are assumed to follow a spring model, i.e., components return to their original position when the force is removed. (c) Force-displacement curve for various shear velocity is measured three times and calibrated with a rigid body at the same velocity according to the same procedure discussed in **Supplementary Note 3**. (d) Crack initiation and propagation energy for different shear velocities are calculated. As the shear velocity increases, crack initiates at smaller displacement but its initiation energy is negligible compared to the crack propagation energy. Crack propagation energy on the other hand is not proportional to the shear velocity and its value varies within the error of the experiment.

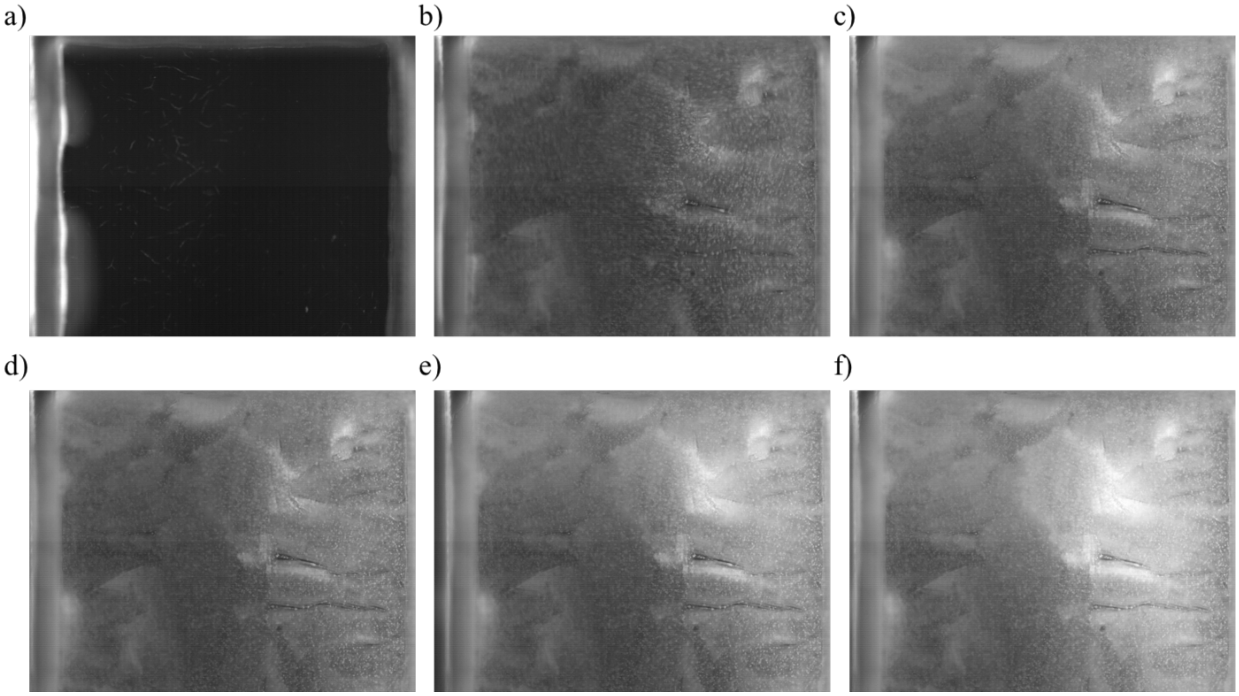

Supplementary Figure 4. High speed imaging. (a) As-poured water inside the cuvette. (b) Frozen cuvette before applying force. This frame is the reference plane for the attached part. (c) 3 ms after applying force from topside, a slight color change is visible. (d) 10 ms and (e) 20 ms after crack inception. (f) 57 ms after crack inception and the ice cuvette is completely detached from the FCS sample.

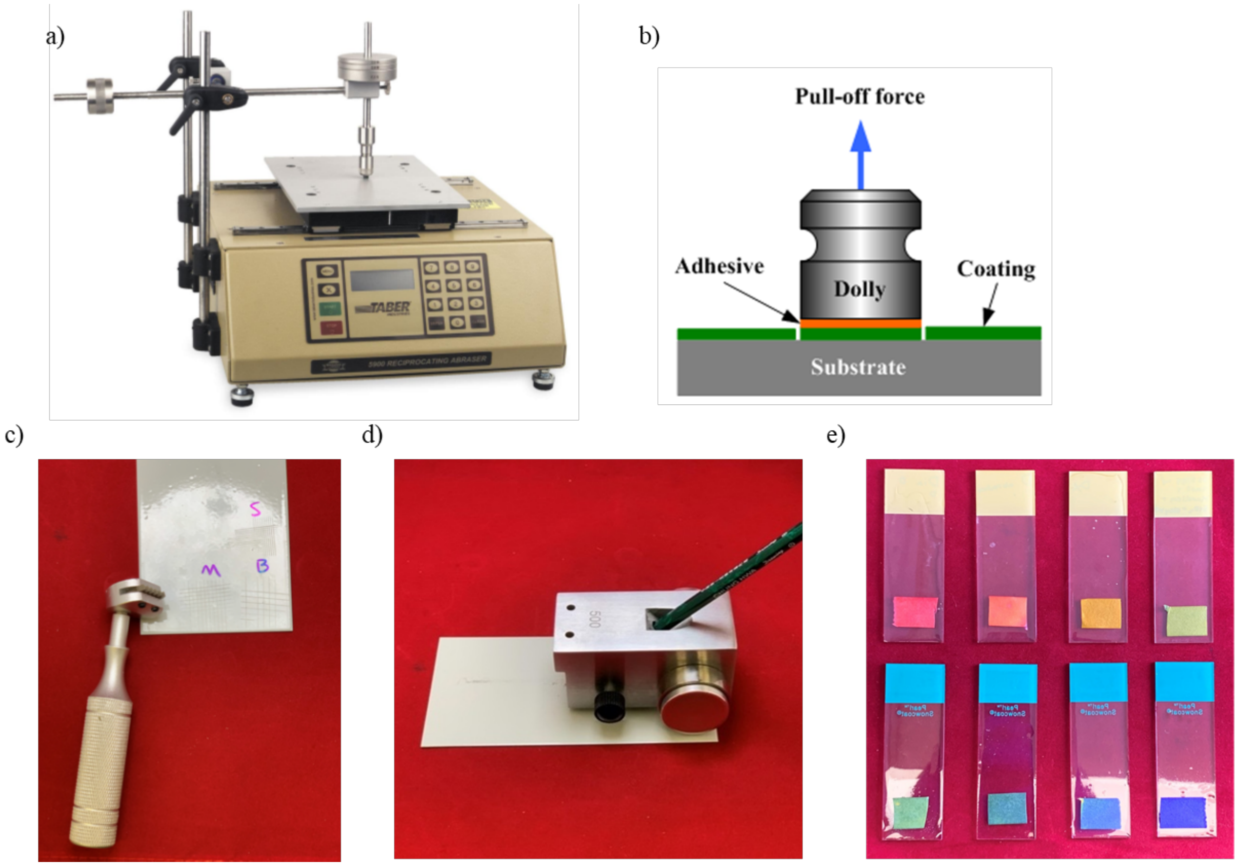

Supplementary Figure 5. Experimental setup for mechanical durability tests. (a) Experimental setup for abrasion metrology ASTM D4060 (b) Pull-off adhesion measurements according to standard ASTM D4541 (c) Cross-hatch measurements according to standard ASTM D3359 (d) Pencil hardness measurements according to Standard ASTM D3363. (e) Samples for chemical durability tests were exposed in a range of pH from 3 to 11. No changes in properties of the coatings were observed.

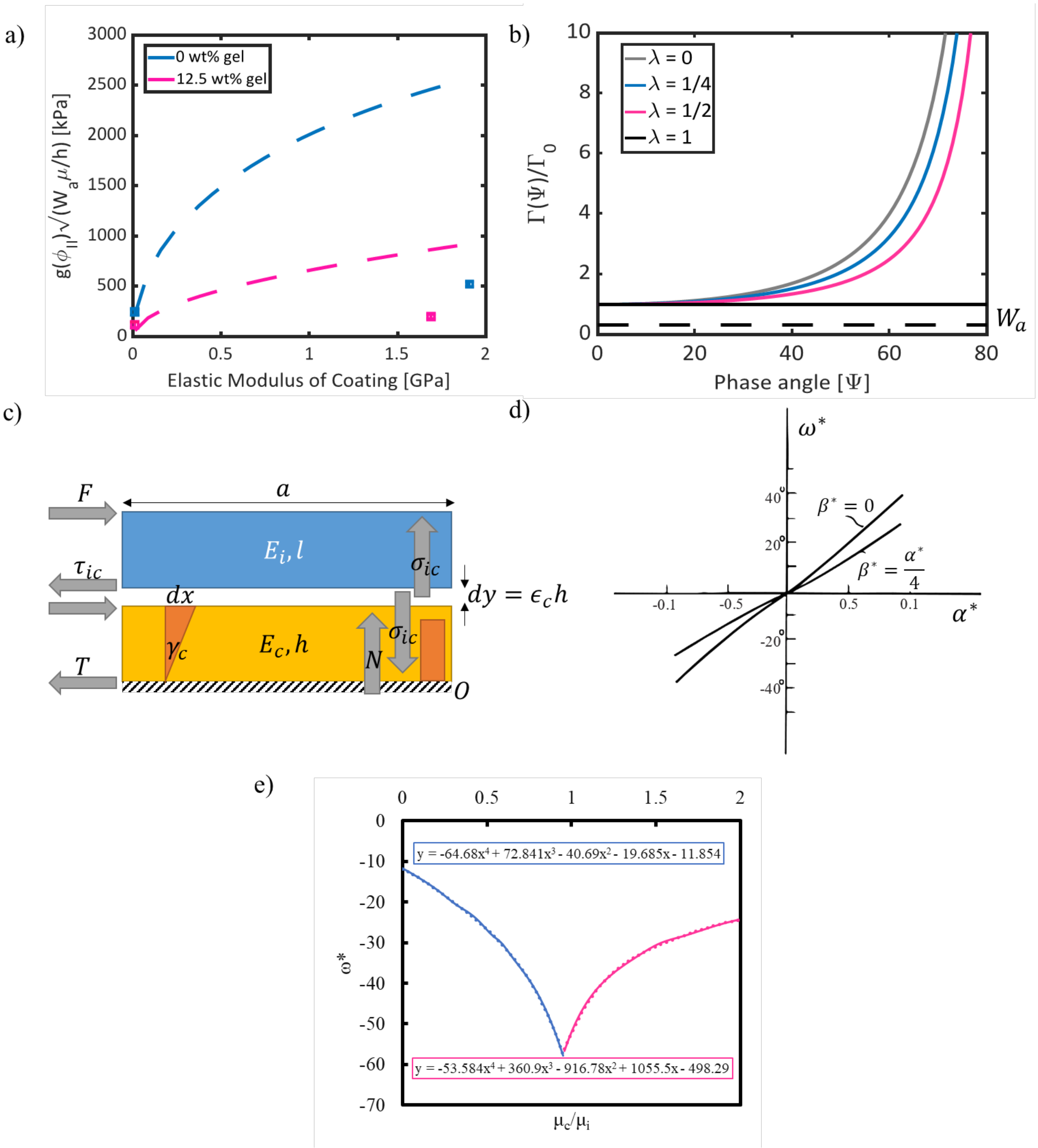

Supplementary Figure 6 Theoretical graphs (a) Ice adhesion strength by considering only thermodynamic work of adhesion for various coatings (b) Ratio of interfacial crack resistance energy for different elastic modulus ratios of coating and ice. It shows that when there is elasticity match between the two materials, the crack energy is independent of the phase angle (i.e. loading condition) and has its minimum value (c) Schematic used to calculate the relation between external force applied and shear strain of the coating. Bending torque for point O is used to evaluate the relation between shear strain at the interface and the applied load. Thus, only bending force is applied by τ_{ic} which is essentially equal to $\beta\frac{F}{a}$, the shear contribution of external force at the interface. (d) This diagram is reproduced[6] in order to find $\omega^*$and consequently finding the phase angle Ψ. (e) Polynomial curve fitting of ω^* for various shear modulus ratio of ice and coating.

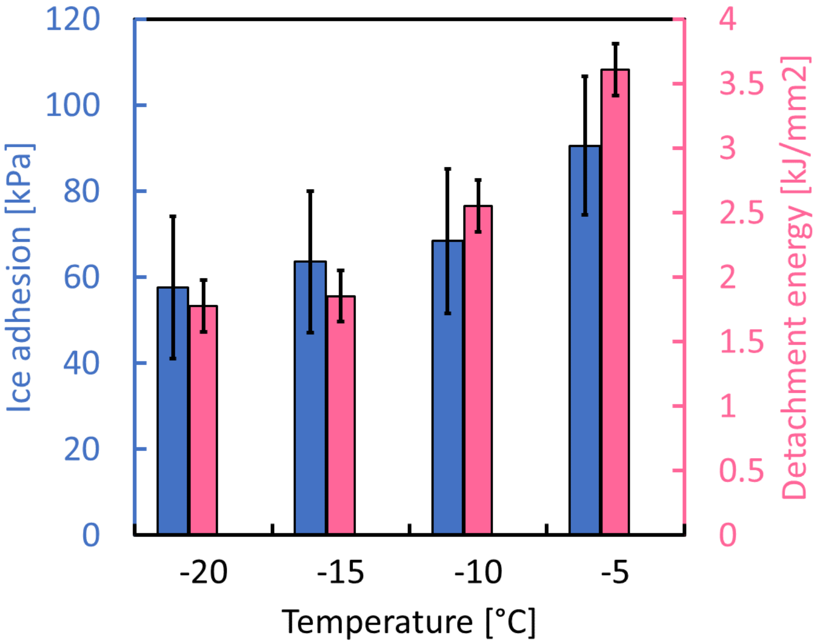

Supplementary Figure 7. Ice adhesion strength and detachment energy at different temperatures. FCS material presented in this work has the best performance for temperatures less than -15 °C as the elastic modulus of the ice and the designed material closely matches. However, at lower temperatures, the ice adhesion strength and detachment energy are slightly higher due to the change of elastic modulus of ice and the material in this temperature range.

Supplementary Notes

Supplementary Note 1. Sample preparation

In order to develop ice shedding surfaces, Polyisocyanate resins were provided by Covestro, and hydrophobic silica R8200© was provided by Evonik. Sylgard 184 was purchased from Dow Chemicals and reagent grade xylene was purchased from Sigma. PDMS gel is prepared by first mixing Sylgard 184 base and hardener at a 1:10 ratio, followed by adding 100 parts of Xylene. Afterwards, the final clear solution is placed in an oven at 120 degrees Celsius for five hours. First, the gel must be crushed into microparticles with a heavy duty blender containing a 1:1 weight ratio of additional Xylene, followed by ultra-sonication until the viscosity drops to 10 cst. The Polyisocyanate resin is loaded with 10 wt% hydrophobic silica and mixed until it becomes homogeneous. Finally, 20 wt% of the PDMS gel in solvent is added to the resin **Fig. S1a**. Aluminum substrates and silicon wafers are sprayed with the material until a 4 mil (100 μm) thick coating is achieved **Fig. S1b**. As shown in **Fig. S1c** the static water contact angle of the sample is measured in order to assess the surface energy. **Fig. S1d** shows the contact angle hysteresis on the surface as 50.7° for receding and 80.2° for advancing contact angle. The optimum value of silica (10 wt%) is calculated based on **Supplementary Note 10** in order to match the elastic modulus of the composite coating to elastic modulus of the ice by rule of mixtures.

Supplementary Note 2. Surface topography of sample

Scanning probe microscopy (SPM) is used to characterize the surface of fracture-controlled surfaces. **Fig. S2a** shows the surface morphology of the sample. Phase III (hydrophobic silica nanoparticles) is seen to cover the phase II (PDMS gel particles). The deformation of the AFM tip retracting sample **Fig. S2b,** shows higher deformation on silica particles compared to the rest of the surface. This is due to the higher shear modulus of the silica vs. that of the polymer matrix. Because the silica particles are located on top of the gel-rich sites (which are responsible for crack nucleation at the interface due to their minimal ice adhesion strength), the higher shear modulus of the silica particles promotes crack propagation instead of increasing the ice adhesion. The adhesion and dissipation maps in **Fig. S2c** and **S2d** are both in agreement with the idea that there should be minimal energy dissipation and adhesion at the interface between phase III and the ice to promote rapid crack propagation.

Supplementary Note 3. Force-displacement calibration

To determine the force versus strain curves of each coating, one must eliminate the effect of displacements of other parts of the setup (e.g., substrate, force gauge bar). A cuvette of the same size should first be attached to the aluminum substrate and set on a cold plate same as **Fig. S3a**. **Fig. S3b** shows the force-displacement curve for the detachment of aluminum substrate from cold plate. This curve could be used to calibrate the detachment of the ice cuvette from the coating in order to isolate the strain at the ice-coating interface. **Fig. 1b**.

Fig. S3c shows the effect of shear velocity on force-displacement curves. Once we increase the shear rate from 1 mm/s to 3 mm/s, ice adhesion on FCS increases which is also observed in Regulagadda et al.[1]. However, the effect of shear velocity on the energy for crack initiation and growth is minimal, **Fig. S3d**. The total detachment energy for FCS is two orders of magnitude lower than that of single-phase polymeric matrix, **Fig. 1d**. This indicates the effect of shear rate on the nature of ice detachment from FCS is insignificant.

Supplementary Note 4. High-speed imaging of ice detachment

FCS demonstrated a significantly faster crack growth rate at the interface than other surfaces **Supplementary Video 1-3**. Using high-speed imaging (Phantom V711), the detachment mechanism of those surfaces was precisely distinguished **Fig. S4**. Using an image processing algorithm, we were able to illustrate the detached region and the crack propagation front accurately **Fig. 2c**. For the final image, a 3D matrix is used with three layers of depth for saving the RGB values, and x-y plane for saving the pixel intensity, and changes in the color intensity for each frame are saved to the corresponding final matrix. To achieve better visibility, all coatings were coated with a black primer, thus the color intensity of specific pixels will increase when the ice forms. Additionally, when the ice is detached, the intensity will increase further. Essentially the difference between the image of liquid and frozen water in the cuvette is used as the reference frame for the sequence. As the force gauge begins to push the cuvette and a detachment front develops, the intensity difference values of consecutive frames are stored in a target matrix in different planes of third dimension to show the red color for the detached area. What we have shown in **Fig. 2c** is the brief outcome of this code in specified timeframes.

Supplementary Note 5. Ice adhesion metrology

Irajizad et al.[3] provided a standard procedure for ice adhesion measurements to avoid discrepancy in the reported ice adhesion measurements. Ice shedding materials are placed on a cold substrate that is connected to a circulating chiller. A k-type thermocouple is used to measure the temperature of the ice shedding material on its surface to ensure that it is at -15 degrees Celsius. A cuvette of 15 mm x 15 mm is placed on the ice-shedding material as shown in **Fig. S3a**. The cuvette is filled with de-ionized water and was allowed to freeze completely. In order to remove the formed ice cube from the substrate, a force gauge (IMADA, model DS2-110) was mounted on a mobile platform and moved towards the cuvette at a rate of 1 mm/s. Ice adhesion strength is calculated by dividing the peak force by the ice-material cross-section. The reported values are an average of twenty (20) measurements on each sample.

Supplementary Note 6. Metrologies for Mechanical durability

A coating's long-lasting icephobic properties is one of the most important characteristics for application in industries such as aerospace, marine, energy, and other industrial/commercial uses. Originally, icing/deicing cycles were used as a measure of the durability of surfaces. There are, however, other important characteristics of the coatings that need to be probed, including their abrasion resistance, the coating hardness, adhesion to substrate, and their ability to withstand harsh environmental conditions. **Supplementary Note 7-9** describe various durability tests that were conducted on FCS samples. The result is shown in **Fig. 3 b-d** in the manuscript.

Supplementary Note 7. Mechanical durability tests

Taber Abrasion:

The Taber abrasion instrument is shown in **Fig. S5a**. Two types of tips were used for these tests: CS-10, a soft tip and H-18, a hard tip. For materials with low durability, the soft tip should be used, as the hard tip will abrade the surface in only a few cycles. The number of cycles could vary from less than ten (10) cycles up to 10,000 cycles depending on the durability of the material. Once abraded, the reduction in the thickness of the material in the abraded area is measured through surface profilometer and is reported. These experiments are conducted at room temperature.

Pull-off Adhesion:

The pull-off test was conducted according to ASTM D4541 with the adhesion meter (PosiTest ATA, Defelkso), **Fig. S5b**. A test dolly with a diameter of 20 mm is glued to the coated surface using epoxy. The glue was allowed to completely cure for at least 24 hours at ambient temperature. Once cured, a perpendicular force was applied to the dolly and the peak force was measured. The type of failure (adhesive vs cohesive) and the pull-off force was recorded. Our measurements were conducted by coating aluminum substrates with FCS material and a MIL-PRF paint as a control, and adhering three dollies to each sample. The pull-off adhesion of the control was measured 7.7±0.5 MPa as a control. An average adhesion strength of 5.1±0.4 MPa was recorded for the FCS sample. The results indicate that FCS is comparable to commercially available paints in terms of adhesion to the underlying substrate.

Cross Hatch:

The experimental setup for these measurements is shown in **Fig. S5c**. An aluminum coupon was coated with state-of-the-art ice-shedding coatings to a thickness of 150 µm. A cross hatch test was done according to ASTM D3359. The tool was placed on the substrate and enough pressure was applied to ensure that all the cutter tips penetrate the test substrate. According to the standard, the spacing between the blades of the cross-hatch tool varies based on the thickness of the coating. The suggested spacing for different thicknesses is: 1 mm spacing tool for coating with thickness in the range of 0-50 µm; 2 mm spacing tool for coating with thickness in the range of 50-100 µm, and a 3 mm spacing tool for coating with thickness in the range of 100-250 µm. The tool was moved on the substrate to develop arrays of 25.4 mm cutline on the coating. The procedure was repeated with a second cut perpendicular to the first lines. With the classification provided by the ASTM D3359, the various ice-shedding materials were compared. In this classification, 5 represents 0% removal area, 4 denotes <5% removal area, 3 stands for 5-15% removal area, 2 classifies 15-35% removal area, 1 represents 35-65% removal area and 0 is assigned for >65% removal area.

Pencil Hardness:

The experimental setup for these measurements is shown in **Fig. S5d** according to standard D3363. A range of standard test pencils from 6B to 6H is used in this metrology. Starting from the hardest pencil, 6H, the pencil is placed on the ice-shedding material and is moved over the surface while pushing downward firmly. The procedure is repeated for all the pencils in the order from 6H to 6B. Scratch hardness is defined as the hardest pencil that will not rupture or scratch the film. The state-of-the-art ice-shedding surfaces after pencil hardness test are shown in **Fig. 4a.**

Supplementary Note 8 Environmental tests

Water Jet:

In this metrology, the FCS was placed under a water jet as shown in **Fig. 4b**. The surfaces were kept for 10 mins under the water jet at 20° angle, and the surface of the samples was visually examined before and after the test **Supplementary Video 4**. No visible change was detected on the FCS samples. This test was used to pre-qualify the coatings for the rain erosion metrology.

Rain Erosion:

This test is conducted by an independent third party, a tier one aerospace OEM. These tests are conducted on standard aluminum airfoils, and three (3) airfoils are chosen for this test to have statistically consistent evaluation. Initially, the leading edge of the airfoils are masked with a tape as shown in **Fig. 4c**. The coating is applied to the remaining part of the airfoils using a spray coating approach. The taping of the leading edge is a required step to ensure impact of the rain droplet at the interface of coated-uncoated section (i.e. interface of the coating-substrate) to simulate harsh delamination conditions. Once the coating is cured, the samples are kept for 24 hours in water at room temperature before assembling on the rain erosion test setup. The rain erosion setup was a whirling arm type setup. The water droplets sprayed on the airfoils with the flow rate of 0.25 m3/hr to achieve 7-10 cm of rainfall per hr. The size of the droplets are 1-4 mm which are simulated through 5 water nozzles. The determined impact speed of the rain droplets on the coating is 172 m/s and the test is conducted at ambient temperature. The test is conducted for 30 mins. The picture of airfoils after the rain erosion test is shown in **Fig. 4c**. The results indicate that the coating is intact after 30 mins with no sign of delamination or any small defect.

Supplementary Note 9. Chemical durability metrology

Approach 1: In these tests, initially fluids with a range of pH (2.49-13) were developed. The acidic solutions were prepared using various concentrations of HCl and water. The basic solutions were made with different concentrations of DI-water and sodium hydroxide. The coated samples were soaked in these solutions for 24 hours and after this time, the integrity of the coatings was examined. **Fig. S5e**

Approach 2: In these tests, specifically designed for aerospace applications, the durability of the coating is examined with respect to hydraulic fluid and lubricating oil. The samples were Aluminum 2024 (T3 temper) by dimension of $152.4 \times 76.2 \times 0.5\ mm$. The samples were coated with primer with the thickness of 25 μm and a coating with thickness of 50 μm. Initially, the samples were immersed in the jet hydraulic fluid at 66 °C for 24 hrs. The coupons were tested before and after the immersion. Only a small staining was observed after the test duration. No visible softening or blistering was detected. In the next set of experiments, the panels were immersed in the lubrication oil at 121 °C for 24 hrs. No visible softening or blistering was observed after the test duration.

Supplementary Note 10. Ice adhesion strength prediction

Since the introduction of the first stress localized surfaces, the choice of matrix remained a challenge. Using a soft second phase into a more durable matrix phase provided the opportunity to achieve a durable coating, however changing the matrix from silicone-based elastomers (E ~ 1-10 MPa) to polyurethane and epoxy resins (E ~ 10-1000 MPa) would always increase the ice adhesion significantly. The predicted ice adhesion value by the previous theory developed for elastomers[2–4] suggests higher ice adhesion for higher shear modulus coatings, **Fig S6a** which is completely inconsistent with the experimental results. One can address the significant difference between the theoretical and experimental values by practical work of adhesion between two surfaces and the mode mixity of the applied load. Volinsky et. al.[5] suggested the difference between thermodynamic work of adhesion and practical work of adhesion ($W_{p,a}$). In this case, dissipated energy at the interface should be considered. When the interfacial fracture is taking place, work of plastic deformation at the crack tip (W_p) is the main reason for the difference between the thermodynamic work of adhesion (W_a) and practical work of adhesion ($W_{p,a}$)[6]

$$W_{p,a} = 2W_a + W_p \tag{1}$$

Interfacial resistance for crack growth Γ has the same physical meaning as $W_{p,a}$. As described by Volinsky et. al.[5], Γ is a function of thermodynamic work of adhesion, elastic properties of ice and coating (λ), and loading condition (phase angle Ψ).

$$\Gamma = \Gamma_0(W_a)(1 + (1 - \lambda)\tan^2 \Psi) \tag{2}$$

Fig. S6b illustrates the effect of phase angle (Ψ) on Γ.Since Γ_0 is the normal contribution of crack growth resistance, one can suggest that its value can find by normal contribution of practical work of adhesion

$$\Gamma_0 = \left(W_{p,a}\right)_n = 2W_a + W_{p,0} \tag{3}$$

Where $W_{p,0}$ is the contribution of energy dissipated due to the plastic deformation at the interface in the pure opening mode. Such term is also suggested to be a function of thermodynamic work of adhesion[5], thus we consider it as

$$W_{p,0} = C_1 W_a \tag{4}$$

Furthermore, one can show the C_1 is much smaller than 1. That is, the plastic work in the orthogonal direction to the interface involves the plastic deformation either in the ice or the coating rather than increasing the crack length at the interface. There are three scenarios when the ice detaching from the surfaces and all result in minimal plastic deformation in the ice and coating:

1- The interface is not brittle but both ice and material have higher yield stress than the maximum applied force thus neither fall into plastic region before detachment of the ice $C_1 = 0$.
2- Non-elastomeric coating that has much lower elastic modulus and yield stress than the applied force and essentially goes under plastic deformation before ice detachment, which

in that case the area under stress-strain curve has to be much smaller compared to W_a itself which requires $\frac{W_{p0}}{W_a} \ll 1 \rightarrow C_1 \ll 1$.

3- Brittle interface or elastomeric material which does not undergo plastic deformation and thus the $C_1 = 0$.

It must be noted that this assumption does not exclude the "plastic work of adhesion". Rather, the work done at the interface in the opening mode is mainly driven by the thermodynamic work of adhesion. Therefore, the "Practical work of adhesion" is determined by the thermodynamic work of adhesion, the relative elastic properties of the coating and ice, and the phase angle. The total strain energy stored in the system[5] can be rewritten as the following equation.

$$W_t - W_e = 2W_a(1 + (1 - \lambda)\tan^2\Psi) \tag{5}$$

On the other hand, the work done by the external force to the system could be calculated by considering the small displacement of the system. When the force F applied at a plane at distance l from the surface, we can write the strain energy stored in the system for small displacement as:

$$W_t - W_e = \beta\frac{F}{a^2}.dx + \alpha\frac{F}{a^2}.dy = \sigma_s\, h\,(\beta\gamma + \alpha\epsilon) \tag{6}$$

$$dy = h\epsilon\,, dx = h\gamma$$

where σ_s is called the ice adhesion stress and can be measured from the experiment using[4] $\frac{F}{a^2}$, h and a are the thickness of the coating and the size of the ice cuvette respectively, and $\alpha = \frac{1}{1+\tan\Psi}$ and $\beta = \alpha\tan\Psi$ are normal and shear components of the force at the interface. The $(-W_e)$ term indicates the energy stored in the ice-material interface before the crack initiation. Our experiments, **Fig. 1d** in the manuscript, indicates that this value is two order of magnitude smaller than the W_t. The bending moment for a system consisting of two bodies constrained by a rigid substrate can be determined based on **Fig. S6c**

$$\beta\frac{F}{a^2}.h = \frac{E_c\gamma h^2}{a^2} \tag{7}$$

In order to simplify the problem, we assume that perpendicular displacements dx and dy at the interface are proportional to respective interfacial stresses σ and τ **Eq. 8,** and isolating γ for σ_s **Eq. 9**

$$\frac{\epsilon h}{\gamma a} \sim \frac{\sigma}{\tau} = \tan\Psi \rightarrow \frac{\epsilon}{\gamma} = \frac{a}{h}\tan\Psi \tag{8}$$

$$\gamma = \frac{\beta a}{E_c h}\sigma_s \tag{9}$$

By plugging **Eqs. 8** and **9** in **Eq. 6** work done by external force can also be written as:

$$W_t - W_e = \frac{\sigma_s^2 h}{\mu_c}\left(\frac{a}{h}(\beta^2 + \alpha^2\frac{a}{h})\right) \tag{10}$$

One can find the equation for ice adhesion stress based on material properties of ice and coating and loading condition by replacing strain and practical work of adhesion in the interfacial crack growth resistance equation and finally isolating the σ_s

$$\sigma_s = \xi \sqrt{\frac{2W_a\mu_c}{h}} \tag{11}$$

$$\xi = \sqrt{\frac{4(1+(1-\lambda)(1+\tan\Psi)^2)}{\left(\frac{a}{h}\right)^2 \frac{1}{\tan^2\Psi} + \frac{a}{h}}}$$

When there is a low shear modulus phase II in the coating, a stress localization function can be added:

$$\sigma_s = \xi g(\varphi_{II}) \sqrt{\frac{2W_a\mu_c}{h}} \tag{12}$$

Where $g(\varphi_{II}) = \frac{1}{\sqrt{\alpha+\beta f(\varphi_{II})\frac{a^2}{l^2}}}$ is the stress localization function[4], α and β are the contribution of the normal and shear stress respectively, and f is the volume fraction of phase II. Interestingly, when there is elasticity match between the ice and coating, increase in the shear component of the stress at the interface enhances the stress localization around the gel-rich sites as well. According to this theory, coatings with two orders of magnitude higher shear moduli can be developed while having low ice adhesion strength.

Supplementary Note 11. Phase angle calculation

The Dundurs parameters[7] α^* and β^* for plane strain are:

$$\alpha^* = \frac{\frac{\mu_i}{\mu_c}(1-v_c) - (1-v_i)}{\frac{\mu_i}{\mu_c}(1-v_c) + (1-v_i)} \tag{13}$$

$$\beta^* = \frac{1}{2}\frac{\frac{\mu_i}{\mu_c}(1-2v_c) - (1-2v_i)}{\frac{\mu_i}{\mu_c}(1-v_c) + (1-v_i)} \tag{14}$$

With these parameters, phase factor ω^* can be found from **Fig. S6d.** In order to get a better understanding of how ω^* changes as a function of $\frac{\mu_c}{\mu_i}$, we have shown a polynomial fit for $\nu_i = \nu_c = \frac{1}{3}$ and various μ_c in **Fig. S6e**. Phase angle Ψ is then defined as

$$\Psi = \tan^{-1}\left(\frac{Fh\sin\omega^* - 2\sqrt{3}M\cos\omega^*}{Fh\cos\omega^* + 2\sqrt{3}M\sin\omega^*}\right) \tag{15}$$

Where F is the applied force and M is the applied torque to the system. In current work, the only torque applied to the system is because of the force F at distance l, $M = Fl$, thus one can find Ψ independent of magnitude of the applied force with respect to the loading condition, distance l, coating thickness h, and respective elastic properties of the ice and coating in ω^*:

$$\Psi = \tan^{-1}\left(\frac{h\sin\omega^* - 2\sqrt{3}l\cos\omega^*}{h\cos\omega^* + 2\sqrt{3}l\sin\omega^*}\right) \tag{16}$$

Supplementary Note 12. Effect of temperature on ice adhesion

The effect of temperature on ice adhesion strength and detachment energy, the total energy of crack initiation and crack propagation, has been measured, **Supplementary Figure 7**. The results indicate that temperature can slightly affect the ice adhesion. In the temperature range of -5 to -20 °C, the shear modulus of ice only varies by around 3 % (0.1 GPa variation compared to 3.0 GPa, shear modulus of ice). This fact can also be checked by the results in which temperature variation did not affect the ice adhesion significantly. However, we expect large variation of material properties with temperature could ultimately affect the ice adhesion.

References

1. Regulagadda, K., Gerber, J., Schutzius, T. M. & Poulikakos, D. Microscale investigation on interfacial slippage and detachment of ice from soft materials. *Mater. Horizons* **9**, 1222–1231 (2022).
2. Chaudhury, M. K. & Kim, K. H. Shear-induced adhesive failure of a rigid slab in contact with a thin confined film. *Eur. Phys. J. E* **23**, 175–183 (2007).
3. Griffith, A. A. Philos Trans R Soc London. in *Ser A* vol. 221 163–198 (1921).
4. Irajizad, P. *et al.* Stress-localized durable icephobic surfaces. *Mater. Horizons* **6**, 758–766 (2019).
5. Volinsky, A. ., Moody, N. . & Gerberich, W. . Interfacial toughness measurements for thin films on substrates. *Acta Mater.* **50**, 441–466 (2002).
6. Wang, C. H. *Introduction to Fracture Mechanics.* (1996).
7. Hutchinson, J. W. & Suo, Z. Mixed Mode Cracking in Layered Materials. *Adv. Appl. Mech.* 63–191 (1991) doi:10.1016/S0065-2156(08)70164-9.